

Efficient sympathetic cooling in mixed barium and ytterbium ion chains

Tomasz P. Sakrejda,* Liudmila Zhukas, and Boris B. Blinov

Department of Physics, University of Washington, Seattle, Washington 98195, USA

(Dated: September 5, 2018)

We Doppler cool barium ions in mixed barium-ytterbium chains confined in a linear RF trap and measure the motional average occupation quantum numbers of all radial normal modes. The full set of orderings in a chain of two barium and two ytterbium ions have been probed, and we show that the average thermal occupation number for all chain configurations strongly depends on the trap aspect ratio. We demonstrate efficient sympathetic cooling of all radial normal modes for the trap aspect ratio of 2.9.

PACS numbers:

I. INTRODUCTION

Scalable quantum computing with trapped atomic ions requires keeping the ions near the quantum motional ground state during the entire computation[1]. Direct laser cooling of the qubit ions cannot be applied as it involves spontaneous emission. Further, Bell-measurement schemes for remote entanglement[2, 3] involve resonant excitation, and crosstalk between the ions used for remote entanglement and their neighbors leads to decoherence. In a mixed-species chain [4, 5], one ion species can be used as the utility species, while the other as the logic species. The former is used for cooling the entire ion chain and for remote entanglement generation, and the latter is used for local quantum information storage and manipulation.

Tight focusing of the relevant laser beams can limit the processes to subsets of ions, but beam quality must be very high to keep crosstalk low enough for practical computation. Alternatively, in a mixed species scheme, one ion species (the “logic” species) is used for information processing while the other species (the “utility” species) is used to perform the dissipative operations. Because of large spectral separation, the logic species’ internal states are unperturbed even if light that is resonant with the utility species is shone on the entire chain.

Same-element mixed species schemes using differing isotopes have been proposed [6–8] as well as cooling only some ions in the chain[6], but off-resonant scattering of the cooling laser light by the logic species is significant[9][10], so species with large spectral shifts are preferable[11]. However, if species of two different elements are instead used, the large mass difference can cause the motion of the two species to become decoupled, which impairs sympathetic cooling and element swapping operations [12]. Barium (Ba) and ytterbium (Yb) atomic ions have a relatively small mass difference of approximately 25%, and thus represent a promising choice of the utility/logic ion pair. For scaling to larger trapped ion quantum processors, ra-

dial modes are preferred to axial modes for local gates [13, 14]. Using radial modes offers several advantages: higher frequencies allow faster gate speeds, addressing chains with lasers perpendicular to the ion chain axis relaxes somewhat the requirements on beam focusing, and gate infidelity due to ions’ thermal motion is reduced by a factor up to $(\frac{\omega_{radial}}{\omega_{axial}})^6$, where the ω ’s are center of mass trap frequencies in the given direction [15].

Unfortunately, mixed species chains’ radial modes are decoupled for typical trapping parameters due to the species’ mass difference [12]. Coupling can be characterized by the largest eigenvector component for each species in a given mode, $\max(\beta_{ij})$, where β_{ij} is the eigenvector component of the j th ion of the species in the i th mode. The coupling is important for both cooling and local quantum gates, as the rate of sympathetic cooling and the speed of the gates both scale as $\max(\beta_{ij})$ [16].

In this paper, we demonstrate efficient sympathetic cooling and good radial vibrational mode coupling in four-ion barium-ytterbium ion chains confined in a linear RF trap. We use Ba⁺ as a thermometer and find that the coupling for each normal mode depends strongly on the trap aspect ratio. In the strongly coupled case, occupation numbers are consistent with the Doppler cooling limit, while in the weakly coupled case the occupation numbers are one to two orders of magnitude higher.

II. THEORY

We measure our chains’ radial motional occupation numbers by measuring the strength of the $\Delta n = 1$ radial motional sidebands of Ba⁺ narrow $6S_{1/2} - 5D_{5/2}$ “shelving” transition near 1762 nm (see Figure 1), relative to the strength of the carrier transition. The Rabi frequency Ω_{ij} for the $\Delta n = 1$ sideband of i th normal mode for the j th ion in the chain is:

$$\Omega_{ij} = \sqrt{n_i + 1} \beta_{ij} \eta_i \Omega_j, \quad (1)$$

where n_i is the radial motional occupation number for the i th mode, β_{ij} is the matrix element of the normal mode eigenvector component for the i th mode and j th ion, η_j is the Lamb-Dicke parameter, and Ω_j is the carrier

*Corresponding author: tomaszs@uw.edu

Rabi frequency (we allow for spatial dependence of the carrier Rabi frequency due to laser beam intensity variation). Each ions' ordering has a different normal mode decomposition, with both different eigenvectors and different frequencies, so a particular order is maintained for the full duration of an experiment.

To estimate normal mode occupation numbers, we calculate the vibrational mode structure of our chains. We numerically calculate the normal mode frequencies and eigenvectors for each unique ordering of the ions in the chain. We find that mode frequencies are clustered in the radial spectrum: modes strongly coupled to barium (ytterbium) motion are near the single barium (ytterbium) radial secular frequency.

To find the radial normal modes frequencies we first consider only the axial direction (z -axis). We minimize the potential energy of the ions to find the equilibrium ion positions in axial direction assuming x and y position of the chain to be zero. One might worry about incorrectly restricting the chain to one dimension, but we can observe and avoid the zig-zag transition in our calculation because it is marked by the softening of the lowest transverse vibrational mode to zero frequency. Once we find the equilibrium positions, we expand the full trap potential around these equilibrium ion positions to find the normal mode frequencies and eigenvector magnitudes.

An example of the numerical calculation for the eigenvector magnitudes as a function of the trap aspect ratio in a chain of two barium and two ytterbium ions is shown in Figure 2. Here the chain order is Ba-Yb-Ba-Yb (BYBY), and we plot the eigenvector magnitudes for the second barium ion x -direction. The strong dependence of the normal mode coupling on the trap aspect ratio can be readily seen. The same trend was observed for all possible chain orders.

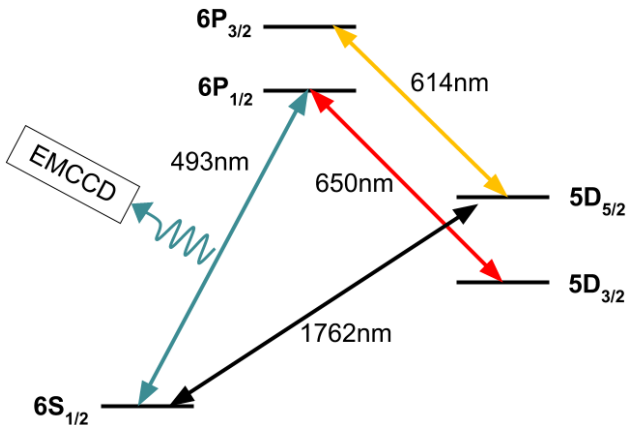


FIG. 1: Ba⁺ energy level diagram. The 493 nm fluorescence from the ions is imaged onto the EMCCD camera. The ion decays from the 6P_{1/2} excited state to the 5D_{3/2} metastable state with a branching fraction of 0.25, and the 650 nm is used to quickly repump from this long-lived state. The 1762 nm laser coherently drives the ion into the 5D_{5/2} state where it is “shelved” and does not participate in the cooling cycle. The 614 nm laser is used to quickly de-shelve the ion.

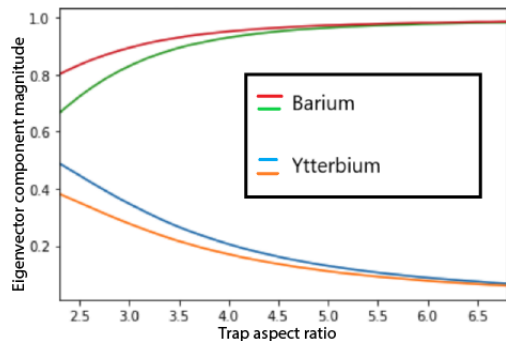


FIG. 2: (Color online) Eigenvector components of one Ba⁺ ion for all four radial modes along the x principal axis of the trap. The left cutoff is the edge of the zig-zag transition. The two normal modes with larger eigenvectors (red and green lines labeled “Barium”) couple more strongly to the barium ion motion, while the two normal modes with smaller eigenvectors (blue and yellow lines labeled “Ytterbium”) couple weakly. As the trap aspect ratio increases, the smaller eigenvector components for this ion decrease leading to even weaker coupling.

To extract the average occupation numbers of different radial modes in the ion chain of N ions, we calculate the transition probability P_j for ion j using the Rabi frequency from eqn. 1, and sum over over both the full occupation number distribution and over all radial normal modes in the spectrum. Assuming thermal state, we have:

$$P_j = \sum_{i=1}^{2N} \sum_{n=0}^{\infty} \frac{1}{\bar{n}_i + 1} \left(\frac{\bar{n}_i}{\bar{n}_i + 1} \right)^n \sin^2(\Omega_{ij}t/2), \quad (2)$$

where \bar{n}_i is the given mode’s average occupation number, and t is the 1762 nm laser exposure time.

III. APPARATUS

The mixed species chain measurements are carried out in a linear RF trap similar to that described in [17]. Species-selective photoionization techniques are used to load both ¹³⁸Ba⁺ and ¹⁷⁴Yb⁺, where barium is Doppler cooled on the 6S_{1/2} – 6P_{1/2} transition with a 986 nm Extended Cavity Diode Laser (ECDL) frequency doubled to produce 493 nm light. An applied 5 gauss magnetic field prevents the creation of the dark states. The 6P_{1/2} level decays to the metastable 5D_{3/2} level with a branching ratio of 0.25, so a 650 nm ECDL is used to pump the population out of this state. All relevant transitions and energy levels of Ba⁺ are shown in Figure 1. Ytterbium is not directly laser-cooled, but sympathetically cooled by Coulomb interaction with the cold barium ions in the chain.

All temperature measurements are performed on barium ions using a 1762 nm fiber laser (Koheras Adjustik) stabilized to a Zerodur-spaced reference optical cavity with a free spectral range of 500 MHz and finesse of

1000. A complete description of the apparatus can be found in [17, 18].

While the short-term linewidth of the 1762 nm laser is of order 100 Hz [19], slow frequency drifts result in a 5 kHz linewidth. This is consistent with the locking system being incapable of stabilizing the laser frequency to better than a few kHz, while the laser itself has a narrow linewidth. Our frequency scans take tens of minutes to a few hours and are thus broadened, so features separated by <15 kHz are not well resolved.

The 1762 nm laser is aligned perpendicular to the trap z -axis, and at roughly 45 degrees to the x - and y -axes. Thus, only the radial sidebands are present in the frequency scans. The laser is focused to a 30 μm Gaussian spot size centered at the ion chain, driving all ions with comparable Rabi frequencies. Polarization control of the 493 nm cooling laser beam with a Pockel's cell is used to optically pump barium ions to the same $6S_{1/2}$ Zeeman state at the start of each run. After the 1762 nm laser exposure, we detect the state of each barium ion simultaneously with an Electron-Multiplied Charge-Coupled Device (EMCCD) camera (Andor Luca) by imaging light scattered by the ions on the cooling transition. If the $6S_{1/2} - 5D_{5/2}$ transition took place, then the ion appears dark; otherwise the ion appears bright. At the end of each experimental run, a short pulse of 614 nm laser light from a frequency-doubled ECDL near 1228 nm returns the barium ions to the ground state.

The experimental sequence is as follows. We Doppler cool the barium ions with the 493 nm and 650 nm lasers for approximately 50 ms with the Pockel's cell turned to a high voltage. Then we discharge the Pockel's cell to turn the 493 nm laser polarization to be circular. The switching time of the Pockel's cell is approximately 1 ms, so we wait for 5 ms to ensure full optical pumping. The 493 nm and 650 nm laser beams are then extinguished successively, and a 1762 nm pulse is applied. Afterward, the 493 nm, 650 nm, and Pockel's cell are turned on for 50 ms to read out the states of the barium ions. The experiments are repeated, varying either the frequency of the 1762 nm during sideband scans, or the duration of the pulse during Rabi flop experiments.

During the experiment the chain sometimes spontaneously reorders, due to either background gas collisions or high chain temperature. When we detect reordering, we discard the experimental cycle and re-establish the chain order by performing melting and crystallization cycles induced by shuttering and unshuttering the Doppler cooling lasers.

IV. RESULTS

We perform weak excitation sideband scans over all radial modes of all possible configurations of two barium and two ytterbium ions. The results are summarized in Figure 3. The normal mode decompositions are used to generate the data fits, as the peak frequencies are

the frequencies of the radial eigenmodes, and the relative peak amplitudes on different ions are given by the eigenvector components and the average occupation numbers (see eqn. 2). The 1762 nm carrier Rabi frequency at each ion position is measured in a separate experiment by performing the carrier Rabi flops with a chain of four barium ions.

The first few sets of data (which can be found in [20] and are not shown in Figure 3) indicated the \bar{n} to be 50 to 2000 times higher than the number that corresponds to the Doppler limit for some of the normal modes, which meant that chains under those conditions could not be used successfully for sympathetic cooling or inter-species quantum logic gates. Analysis of that data revealed a correlation [20] between the maximum eigenvector component of the cooled ion species and the measured \bar{n} . Noting the correlation, we search for trap and chain configurations for which the eigenvector components would be large for the cooled species in all modes. Using the numerical normal mode structure calculation tool described in the theory section, we found that lowering the trap aspect ratio from 5.5 (used in [20]) to 2.9 increases the normal mode eigenvector component values above the expected 0.05 "threshold" value regardless of chain ordering. Some chain orderings were found to be better cooled than the others. For example, in the *BY*YB configuration, the maximum eigenvector component is at least 30% lower than the maximum eigenvector component in any other configuration.

We summarize our measurements of the radial mode \bar{n} as a function of the maximum eigenvector component for both the old set [20] and the new set of data in Figure 4. We find very large reduction in \bar{n} for maximum eigenvector component above approximately 0.05. These values of \bar{n} correspond to normal mode temperatures between the Doppler limit for a single trapped barium and about 40 times the Doppler limit. These values are consistent with technical difficulties of achieving the Doppler cooling limit in a lambda system such as Ba^+ [21]. At low intensities of the cooling and repump lasers, the rate of heating from residual micromotion balances the cooling rate well above the Doppler limit, while at high intensities the combination of power broadening and interference effects between the cooling and the repump transitions causes the minimum temperature to also increase well above the Doppler limit.

V. CONCLUSIONS

We studied the sympathetic cooling of barium-ytterbium chains in a linear RF trap in which only barium is directly laser cooled. We found that reducing the aspect ratio of the trap reduced the measured ion temperature in all normal modes. The ion chain has been cooled from a factor of 50 to 2000 the Doppler limit (well outside the Lamb-Dicke regime) to within a factor of 1 to 40 the Doppler limit, which is consistent with

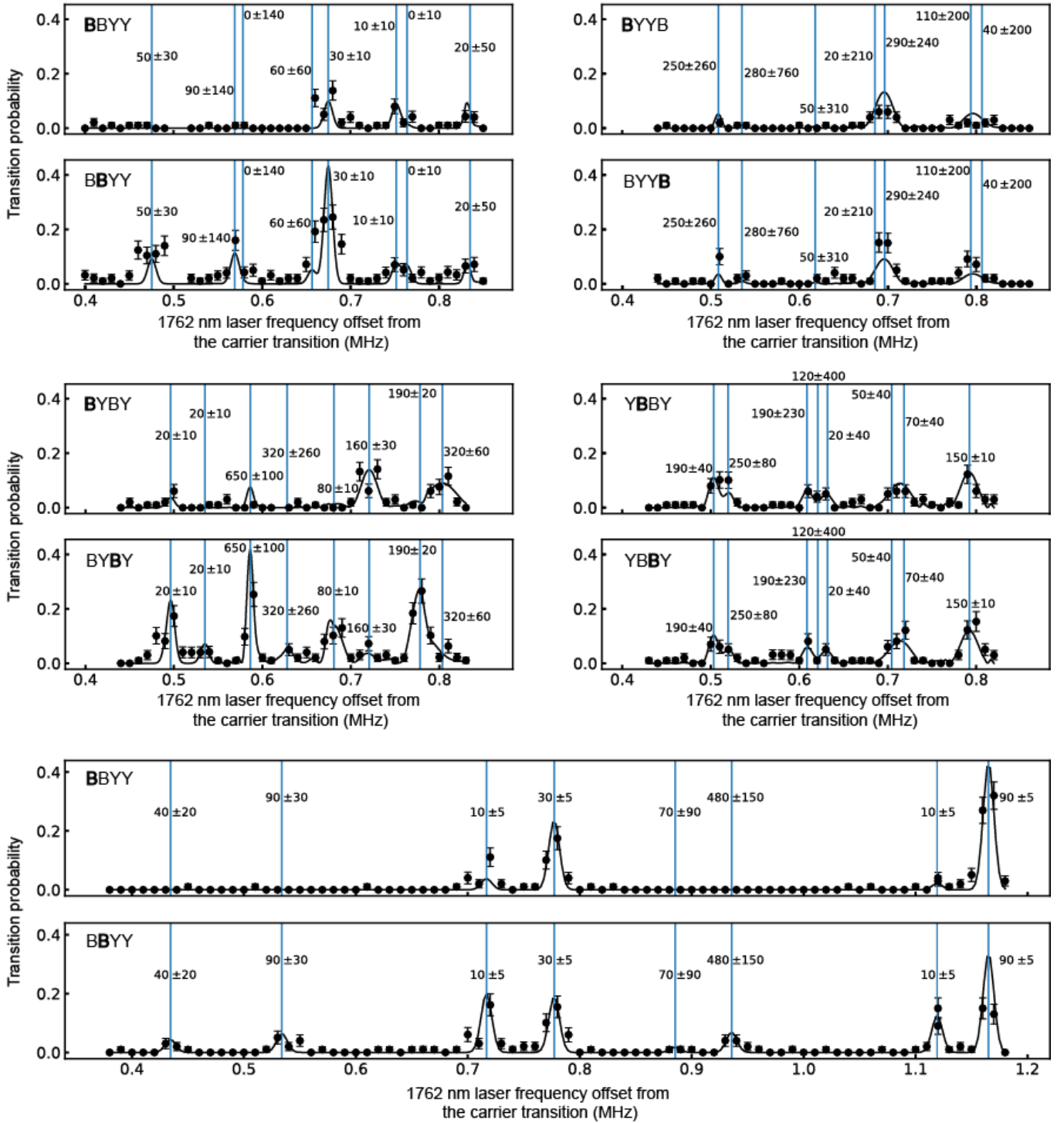


FIG. 3: 1762 nm laser scans showing $\Delta n = 1$ sideband transitions. Two sets of radial mode peaks are present in each scan. Bold font is used to indicate which Ba^+ in the chain the spectrum was taken from. Radial mode occupation numbers are extracted from the peak amplitudes. The vertical lines indicate the calculated frequencies of the normal modes, and the associated radial mode occupation numbers are printed closely. The error bars on the measured occupation numbers are statistical. The Doppler limit for the secular frequency modes between 0.5-0.9 MHz corresponds to an \bar{n} of 16 – 30 for a $^{138}\text{Ba}^+$. The peak sizes are proportional to the associated \bar{n} 's, the eigenvector component β_{ij} 's, and the exposure time, which is not displayed but which is adjusted to stay in the weak excitation regime. In the bottom scan a squeeze potential is applied to the trap's RF rods, which pushes the radial mode frequencies apart and changes the eigenvector component sizes along the two axes.

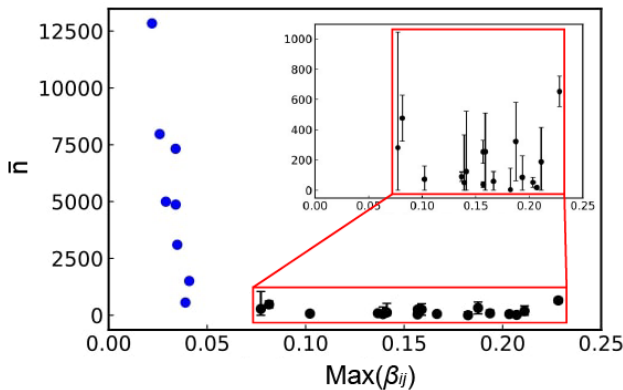


FIG. 4: The \bar{n} values vs maximum eigenvector component. The normal mode occupation number shows threshold-like behavior. All new data in the eigenvector component range $\beta_{ij} > 0.05$, shown in black, were taken at an aspect ratio of 2.9 except for the last set of data in Figure 3 corresponding to the Ba-Ba-Yb-Yb configuration. Data in the range $\beta_{ij} < 0.05$, shown in blue, are taken from [20] and are not presented in Figure 3. These data do not have uncertainty displayed because the measured temperatures are outside the Lamb-Dicke regime.

the cooling limitations in our setup. Our measurements show that the radial normal mode temperature is strongly dependent on the size of the maximum normal mode component of the cooled species. We conclude that in order to achieve efficient sympathetic cooling and interspecies quantum logic gates using radial vibrational modes, traps with lower aspect ratio are desirable.

Acknowledgments

The authors wish to thank John Wright and Wen-Lin Tan for help with earlier parts of the experiments, and Megan Ivory, Jennifer Lilieholm, Alexander Pierce, Ramya Bhaskar and James Walker Steere for helpful discussions. This research was supported by National Science Foundation Grant No. 1505326.

-
- [1] J. I. Cirac and P. Zoller, *Phys. Rev. Lett.* **74**, 4091 (1995), URL <https://link.aps.org/doi/10.1103/PhysRevLett.74.4091>.
- [2] D. L. Moehring, P. Maunz, S. Olmschenk, K. C. Younge, D. N. Matsukevich, L.-M. Duan, and C. Monroe, *Nature* **449** (2007), URL <https://www.nature.com/articles/nature06118>.
- [3] C. Monroe, R. Raussendorf, A. Ruthven, K. R. Brown, P. Maunz, L.-M. Duan, and J. Kim, *Phys. Rev. A* **89**, 022317 (2014), URL <https://link.aps.org/doi/10.1103/PhysRevA.89.022317>.
- [4] V. Rajagopal, J. P. Marler, M. G. Kokish, and B. C. Odom, *European Journal of Mass Spectrometry* **22**, 1 (2016), <https://doi.org/10.1255/ejms.1408>, URL <https://doi.org/10.1255/ejms.1408>.
- [5] J.-S. Chen, S. M. Brewer, C. W. Chou, D. J. Wineland, D. R. Leibbrandt, and D. B. Hume, *Phys. Rev. Lett.* **118**, 053002 (2017), URL <https://link.aps.org/doi/10.1103/PhysRevLett.118.053002>.
- [6] H. Rohde, S. T. Gulde, C. F. Roos, P. A. Barton, D. Leibfried, J. Eschner, F. Schmidt-Kaler, and R. Blatt, *Journal of Optics B: Quantum and Semiclassical Optics* **3**, S34 (2001), URL <http://stacks.iop.org/1464-4266/3/i=1/a=357>.
- [7] K. Sugiyama, *Japanese Journal of Applied Physics* **38**, 2141 (1999), URL <http://stacks.iop.org/1347-4065/38/i=4R/a=2141>.
- [8] B. B. Blinov, L. Deslauriers, P. Lee, M. J. Madsen, R. Miller, and C. Monroe, *Phys. Rev. A* **65**, 040304 (2002), [quant-ph/0112084](https://arxiv.org/abs/quant-ph/0112084).
- [9] D. Hucul, I. V. Inlek, G. Vittorini, C. Crocker, S. Debnath, S. M. Clark, and C. Monroe, *Nature Physics* **11**, 37 (2014), URL <http://dx.doi.org/10.1038/nphys3150>.
- [10] J. P. Home, M. J. McDonnell, D. J. Szwer, B. C. Keitch, D. M. Lucas, D. N. Stacey, and A. M. Steane, *Phys. Rev. A* **79**, 050305 (2009), URL <https://link.aps.org/doi/10.1103/PhysRevA.79.050305>.
- [11] Y. Wang, M. Um, J. Zhang, S. An, M. Lyu, J.-N. Zhang, L.-M. Duan, D. Yum, and K. Kim, *Nature Photonics* **11**, 646 (2017), ISSN 1749-4893, URL <https://doi.org/10.1038/s41566-017-0007-1>.
- [12] J. B. Wübbena, S. Amairi, O. Mandel, and P. O. Schmidt, *Phys. Rev. A* **85**, 043412 (2012), URL <https://link.aps.org/doi/10.1103/PhysRevA.85.043412>.
- [13] Lin, G.-D., Zhu, S.-L., Islam, R., Kim, K., Chang, M.-S., Korenblit, S., Monroe, C., and Duan, L.-M., *EPL* **86**, 60004 (2009), URL <https://doi.org/10.1209/0295-5075/86/60004>.
- [14] S.-L. Zhu, C. Monroe, and L.-M. Duan, *Phys. Rev. Lett.* **97**, 050505 (2006), URL <https://link.aps.org/doi/10.1103/PhysRevLett.97.050505>.
- [15] C. D. B. Bentley, A. R. R. Carvalho, and J. J. Hope, *New Journal of Physics* **17**, 103025 (2015), URL <http://stacks.iop.org/1367-2630/17/i=10/a=103025>.
- [16] D. Kielpinski, B. E. King, C. J. Myatt, C. A. Sackett, Q. A. Turchette, W. M. Itano, C. Monroe, D. J. Wineland, and W. H. Zurek, *Phys. Rev. A* **61**, 032310 (2000), URL <https://link.aps.org/doi/10.1103/PhysRevA.61.032310>.
- [17] M. R. Dietrich, N. Kurz, T. Noel, G. Shu, and B. B. Blinov, *Phys. Rev. A* **81**, 052328 (2010), URL <https://link.aps.org/doi/10.1103/PhysRevA.81.052328>.
- [18] J. Wright, C. Aughter, C.-K. Chou, R. D. Graham, T. W. Noel, T. Sakrejda, Z. Zhou, and B. B. Blinov, *Quantum Information Processing* **15**, 5339 (2016), ISSN 1570-0755, URL <https://doi.org/10.1007/s11128-015-1220-9>.
- [19] T. Noel, M. R. Dietrich, N. Kurz, G. Shu, J. Wright, and B. B. Blinov, *Phys. Rev. A* **85**, 023401 (2012),

- URL <https://link.aps.org/doi/10.1103/PhysRevA.85.023401>.
- [20] J. Wright, Ph.D. thesis, University of Washington (2015), URL http://depts.washington.edu/qcomp/pdfs/John_thesis.pdf.
- [21] G. Janik, W. Nagourney, and H. Dehmelt, J. Opt. Soc. Am. B **2**, 1251 (1985), URL <http://josab.osa.org/abstract.cfm?URI=josab-2-8-1251>.